

System Reliability-Based Design Optimization Under Tradeoff Between Reduction of Sampling Uncertainty and Design Shift

Sangjune Bae

Department of Mechanical and
Aerospace Engineering,
University of Florida,
Gainesville, FL 32611
e-mail: sjune.bae@ufl.edu

Nam H. Kim¹

Professor
Department of Mechanical and
Aerospace Engineering,
University of Florida,
Gainesville, FL 32611
e-mail: nkim@ufl.edu

Seung-gyo Jang

Agency for Defense Development,
Daejeon 305-600, South Korea
e-mail: Jsg4580@add.re.kr

This paper presents a tradeoff between shifting design and controlling sampling uncertainty in system reliability-based design optimization (RBDO) using the Bayesian network. The sampling uncertainty is caused by a finite number of samples used in calculating the reliability of a component, and it propagates to the system reliability. A conservative failure probability is utilized to consider sampling uncertainty. In this paper, the sensitivity of a conservative system failure probability is derived with respect to the design change and the number of samples in a component using Bayesian network along with global sensitivity analysis (GSA). In the sensitivity analysis, GSA is used for local sensitivity calculation. The numerical results show that sampling uncertainty can significantly affect the conservative system reliability and needs to be controlled to achieve the desired level of system reliability. Numerical examples show that both shifting design and reducing sampling uncertainty are crucial in the system RBDO.

[DOI: 10.1115/1.4041859]

Keywords: reliability-based design optimization, epistemic uncertainty, Bayesian network, global sensitivity analysis

1 Introduction

In the reliability analysis or reliability-based design optimization (RBDO), the probability of failure is used to determine the reliability of a design. Due to the complexity of calculation, often an approximation is used. For example, sampling-based methods, such as Monte Carlo simulation (MCS), use a large number of samples to estimate the probability of failure. Unless an infinite number of samples is used, the estimated probability of failure has sampling uncertainty; that is, different sets of samples yield different probabilities of failure [1–3].

In general, different types of uncertainties in the mathematical calculation can be categorized into either aleatory uncertainty or epistemic uncertainty [4]. The aleatory uncertainty represents variability that exists inherently in nature. It is generally considered irreducible. Therefore, it is necessary to take its effect into account in the design. Traditional RBDO expresses aleatory uncertainty using a probability density function (PDF) and calculates the probability of failure due to the uncertainty. On the other hand, epistemic uncertainty represents the uncertainty due to the lack of knowledge or information. Therefore, epistemic uncertainty may not be random but uncertain. In general, the epistemic uncertainty is reducible if additional information or data is available. Sampling uncertainty belongs to this group because the probability calculation becomes more accurate as more samples are provided. Even if there are different opinions on how to represent epistemic uncertainty, it is generally accepted that sampling uncertainty can also be represented using a PDF [5].

There have been approaches to include epistemic uncertainty in reliability analysis [6,7]. When both aleatory and epistemic uncertainties exist, reliability analysis is often performed in a double-loop algorithm, where the inner loop calculates the probability of failure for given aleatory uncertainty, while the outer loop

calculates the distribution of failure probability due to the epistemic uncertainty. These methods successfully reflect the effect of uncertainty on the reliability calculation, and a conservative failure probability is used for RBDO. Likewise, the conservative estimate of failure probability with a specific target conservativeness will be used as a design criterion in this paper.

Once the effect of epistemic uncertainty is quantified, the next question is how to control such uncertainty. Note that the traditional RBDO approach changes design to satisfy the reliability constraints under all uncertainties. However, the traditional RBDO with epistemic uncertainty often yields too conservative designs due to an excessive amount of uncertainty. Instead of compensating for epistemic uncertainty using conservatism, it would be necessary to quantify and reduce the epistemic uncertainty to achieve a meaningful design out of RBDO.

In this paper, among many sources of epistemic uncertainty, only sampling uncertainty is considered, where a normal distribution can approximate the distribution of failure probability. In our previous work, the effect of design perturbation and change in the number of samples is shown on the conservative estimate of a single probability of failure [8,9]. In this paper, the goal is to identify the effect of sampling uncertainty and design change of a component on the system probability of failure (SPF). A system in this paper refers to a group of many components connected. Unlike a typical multidisciplinary system with feedback coupling, this paper assumes that the system is acyclic and can be dissected into a group of independent components, which do not share any input variables with another.

There are numerous methods to estimate the probability of failure. For example, it is possible to approximate the limit state function to a linear or quadratic form (FORM, SORM) [10]. Bayesian reliability approach can also be applied to estimate a small probability of failure [11]. To approximate the distribution of the probability of failure, a kernel density estimation is available [12]. However, limit state function approximation is essentially not accurate enough for probability estimation, and the other methods require additional epistemic uncertainty source to quantify the probability of failure such as bandwidth selection in kernel density

¹Corresponding author.

Contributed by the Design Automation Committee of ASME for publication in the JOURNAL OF MECHANICAL DESIGN. Manuscript received April 12, 2018; final manuscript received October 17, 2018; published online January 11, 2019. Assoc. Editor: Ping Zhu.

estimation. In this paper, it is foreseen that MCS may require a large number of samples for a small probability of failure. However, it is one way to eliminate other sources of uncertainty but the sampling uncertainty.

There are two major mechanisms for propagating uncertainty: (a) the propagation of component probability of failures (CPF) to the system probability of failure and (b) the propagation of epistemic uncertainty in components to the system. The former is equivalent to expressing the system probability of failure in terms of CPFs. There are many methods to calculate the system probability of failure, but a Bayesian network [13,14] is utilized in this paper. The Bayesian network is an intuitive way to understand the relationship among the components because it visualizes the relationship of the component through a directed acyclic graph. Therefore, it is possible to evaluate the contribution of individual components to the system. For the latter, global sensitivity analysis (GSA) will be utilized to show the propagation of the epistemic uncertainties in the components to a system. GSA calculates the effect of the uncertainty in each component failure probability on the uncertainty in the system probability of failure. Details will be explained in Sec. 3.

A Bayesian network has been utilized in design optimization to construct the probabilistic relationship between the input variables and the output response. Such model is exploited as a surrogate model, replacing an expensive computational one [15,16]. Unlike these approaches, this paper shows the tradeoff between the uncertainty reduction and the design perturbation in a Bayesian network.

In this paper, the design sensitivities of a conservative estimate of system probability of failure concerning component design variables and the number of samples in components are presented using the Bayesian network and GSA. Previously, GSA has been used for screening important variables [17]. This paper shows how the global sensitivity analysis can be explicitly incorporated into the design sensitivity.

The paper is composed of seven sections including the conclusions. Section 2 shows two different methods to deal with epistemic uncertainty. Section 3 is a general explanation of Bayesian network and GSA. Section 4 explains how the epistemic sampling uncertainty is reflected in the design sensitivity at the system level. Section 5 exhibits the contribution of this paper by quantifying the effect of sampling uncertainty on the design sensitivity of system failure probability. Section 6 demonstrates how the derived sensitivity can be utilized in RBDO using pyrotechnical mechanical device example.

2 Dealing With Sampling Uncertainty

As stated before, the probability calculation using sampling methods can be affected by the number of samples. When a finite number of samples are used, there is an uncertainty of calculation, which leads to a distribution of probability. In general, there are two ways of considering sampling uncertainty: “living with uncertainty” and “shaping uncertainty.” In this section, these two concepts are explained in the RBDO framework.

Let $h(\mathbf{d}, \mathbf{X})$ be a limit state function (i.e., constraint function) with the vector of design variables \mathbf{d} and the vector of aleatory random variables \mathbf{X} . The event of failure is determined when $h(\mathbf{d}, \mathbf{X}) \geq 0$. When MCS with N samples is used, the probability of failure can be estimated as

$$P_F(\mathbf{d}) = \frac{1}{N} \sum_{i=1}^N I_F(h(\mathbf{d}, \mathbf{x}_i) \geq 0) \quad (1)$$

where $I_F(\cdot)$ is the indicator function, which becomes one if its argument is true; otherwise zero. In Eq. (1), \mathbf{x}_i is the i th sample of random variable \mathbf{X} . Therefore, the aleatory randomness in the variable results in a single value of probability of failure.

However, the estimated probability of failure in Eq. (1) may change if different sets of samples are used. That is, due to

sampling uncertainty, the probability of failure has uncertainty, which can be modeled as a normal distribution $\hat{P}_F \sim N(\mu_F, \sigma_F^2)$, where the mean is $\mu_F = P_F$ and the variance is $\sigma_F^2 = P_F(1 - P_F)/N$ [8]. The sum of the indicator function $NP_F(\mathbf{d})$, approximately follows a normal distribution $\sim N(NP_F, NP_F(1 - P_F))$ when the normality condition is satisfied, such that $NP_F > 10$ and $N(1 - P_F) > 10$ [18]. If the condition is not satisfied, then we cannot assume that the distribution is Gaussian. In such a case, other methods such as the bootstrap method [19] can be used to estimate the variance. Note that the standard deviation σ_F represents sampling uncertainty. When the probability of failure approaches zero, the coefficient of variation considerably increases [9]. In other words, sampling uncertainty becomes significant when the probability of failure becomes small.

One method to deal with such sampling uncertainty for achieving the target probability of failure is to use a conservative estimate of failure probability. Therefore, the reliability constraint can be defined as

$$P_{F,\text{cons}} \equiv P_F + z_{1-\alpha}\sigma_F \leq P_T \quad (2)$$

where $P_{F,\text{cons}}$ is the conservative estimate of failure probability, $z_{1-\alpha}$ is the z-score with the confidence level of $1 - \alpha$, and P_T is the target probability of failure.

Figure 1 illustrates how the reliability constraint can be satisfied when the probability of failure is distributed. Note that the sampling uncertainty causes the distribution. As seen in Fig. 1, there are two ways to obtain a satisfactory design when the reliability constraint in Eq. (2) is violated. The first one is to shift the mean of the distribution, and the second is to reduce the standard deviation, σ_F . Figure 1(a) shows the case when the entire distribution of \hat{P}_F is shifted by perturbing the design variables. The design will satisfy the reliability constraint under both aleatory and epistemic uncertainties. This approach yields a more conservative design to reduce the probability of failure. Since this approach does not reduce but compensates for the epistemic uncertainty by making design conservative, the approach is referred to as “living with uncertainty” in this paper.

On the other hand, instead of shifting the distribution, it is also possible to reduce the epistemic uncertainty to achieve the target reliability. In Eq. (2), the reliability constraint can be satisfied by reducing the standard deviation, as shown in Fig. 1(b). In this case, the design does not change, but only the epistemic uncertainty is reduced, which can be achieved by providing more samples. Because this approach compensates for the epistemic uncertainty by changing uncertainty, it is referred to as “shaping uncertainty” in this paper.

Traditional RBDO focuses on living with uncertainty. However, it often yields too conservative design due to large uncertainty. Therefore, it would be necessary to control the uncertainty to reduce the cost further. For engineering systems, having a conservative design can be safe, but it will cost more during operation. On the other hand, shaping uncertainty can save operation cost, but it will be more expensive in the development stage due to extra samples or tests. Therefore, it should be possible to compare the tradeoff between the two approaches.

3 Global Sensitivity Analysis in Bayesian Network

3.1 System Probability Using Bayesian Network. When a system consists of many components, the SPF, P_F^{sys} , can be determined as a function of the CPF. From CPFs, the SPF can be calculated using the relationships among the components. In this paper, a Bayesian network is used to quantify such relationship. The network uses Bayes’ theorem to calculate the SPF along with conditional probabilities [13,20]. An example of a simple Bayesian network is given in Fig. 2, where $P(A|B)$ is the probability of having event A conditioned on event B. An event can be either success “S” or failure “F.”

The Bayesian network consists of a graphical model called directed acyclic graph and conditional probability tables

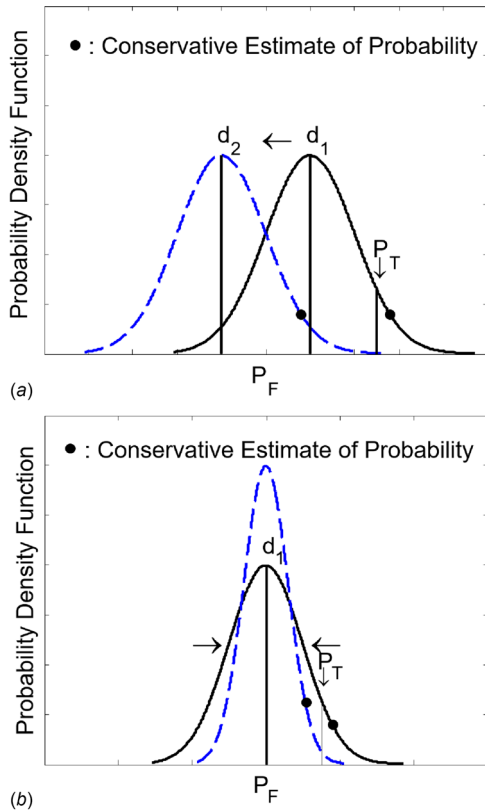


Fig. 1 Options to satisfy reliability constraint with conservative probability of failure: (a) living with uncertainty and (b) shaping uncertainty

associated with it. The circles in Fig. 2 are called “nodes” and represent each component in the system. The arrows, or the so-called causal edges, show the dependence of the components. For example, if the arrow starts from node B and reaches node A as in the figure, then it represents that the probability of node A depends on that of node B. In this case, node B is called “parent node and node A is called “child node.”

The table on the side of a node shows the probabilities of failure of the node conditioned on the parent nodes. For node C in the figure, for example, there are four possible failure cases: node C fails when both A and B succeed, node A succeeds but B fails, node A fails but B succeeds, and both A and B fail. In the table, the conditional probability of failure corresponding to each case is calculated.

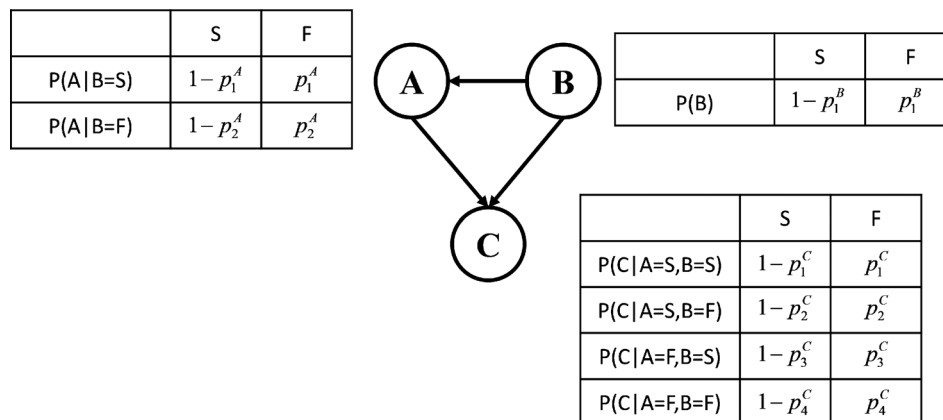


Fig. 2 Example of three-node Bayesian network

Based on this configuration, the SPF can be expressed as a function of CPFs using Bayes’ theorem. The definition of the SPF depends on what the system is, but let us assume that the SPF is defined here as the probability of failing node C, which is the last node in the system. Then, the SPF is calculated based on the Bayesian network as

$$P_F^{sys} = P(C = F) = P_1^C(1 - P_1^A)(1 - P_1^B) + P_2^C(1 - P_2^A)P_1^B + P_3^C P_1^A(1 - P_1^B) + P_4^C P_2^A P_1^B \quad (3)$$

It is noted that the calculation of SPF does not require any computational cost in addition to calculating CPFs. As shown in Eq. (3), a node can have multiple failure scenarios, such as P_1^A and P_2^A , which causes a notational difficulty in the following derivations. Therefore, we will use the following notation to represent CPFs: $\{P_1^A, P_2^A, P_1^B, \dots, P_4^C\} = \{P_F^1, P_F^2, \dots, P_F^m\}$; that is, there are m CPFs. Equation (3) can be generalized to the relationship between SPF and CPFs as

$$P_F^{sys} = P_F^{sys}(P_F^1, P_F^2, \dots, P_F^m) \quad (4)$$

3.2 Uncertainty in Failure Probability Estimation. There are many methods available in calculating the CPFs, such as surrogate-based methods [21] and sampling-based methods [19]. Different methods have their own advantages, but it is out of the scope of this paper to discuss them. In this paper, it is assumed that CPFs are calculated using a sampling-based method. The unique characteristic of sampling-based methods is that the calculated CPFs have sampling uncertainty. That is, the CPF P_F^i is random because different sets of samples may yield different values of CPF. When MCS is used to calculate the CPF as in Eq. (1), the variance in CPF can be calculated as

$$V_F^i \equiv V[P_F^i] = \frac{P_F^i(1 - P_F^i)}{N_i} \quad (5)$$

where N_i is the number of samples used to calculate P_F^i . It means that the CPF has uncertainty due to sampling uncertainty, which can be represented as $P_F^i \sim N(P_F^i, V_F^i)$. An important observation in Eq. (5) is that the uncertainty is a function of the level of probability and the number of samples. Note that V_F^i is inversely proportional to the number of samples used. Therefore, it can be controlled by changing the number of samples.

Since the SPF is a function of CPFs as shown in Eq. (4), its variance can be calculated using the definition of variance [8]

$$V_F^{sys} \equiv V[P_F^{sys}] = E[(P_F^{sys})^2] - E[P_F^{sys}]^2 \quad (6)$$

When the SPF is expressed as a polynomial form of CPFs as in Eq. (3), the variance can be analytically expressed in terms of

CPFs and their variances. When SPF is not in the form of polynomials of CPFs, a bootstrap method can be used to estimate the variance in SPF. For example, the source of failure might be of interest rather than the failure itself. In Fig. 2, it might be of interest to minimize the probability of component A to fail when component C fails. In this case, the conditional probability $P(A = F|C = F)$ becomes SPF, which is not a polynomial. In the bootstrap method, the distribution of CPF is estimated by resampling of function outputs, which results in some samples of CPFs, and then, they are randomly sampled and used in Eq. (4) to calculate samples of SPF from which the variance can be estimated. The detailed explanation of bootstrap method for estimating uncertainty can be found in Bae et al. [8].

As shown before, aleatory randomness in input parameters causes the probability of failure, while sampling uncertainty causes the uncertainty in the failure probability. Similar to CPFs, when the SPF has sampling uncertainty, the reliability constraint can be defined using a conservative estimate of the SPF as

$$P_{F,cons}^{sys} \equiv P_F^{sys} + z_{1-\alpha}\sigma_F^{sys} \leq P_T \quad (7)$$

where the standard deviation of the SPF can be obtained by the square root of the variance in Eq. (6).

3.3 Global Sensitivity Analysis. A major contribution of this paper is to reduce the variance of the SPF in Eq. (6) by considering the number of samples as an input parameter. Since the input parameters such as the number of samples are all defined at the component level, the relationship between the variance of the SPF and the variance in component input parameters needs to be identified. To develop such a relationship, the GSA is utilized in this paper [22,23]. GSA decomposes the variance of a function output into the variance of input variables. If it is applied to the Bayesian network, the SPF can be regarded as the output and the CPF as the input. Therefore, GSA shows the contribution of the variance of CPF to the variance of the SPF. Based on this property, GSA will be used to calculate the sensitivity of the variance of SPF with respect to the variance of CPFs in this paper. The variance-based GSA requires the random input variables to be independent of each other. The components in a BN do not share any aleatory random variables. Therefore, they are all independent of each other. Note that the nodes in a BN are only conditionally independent of its non-descendants given its parents, while CPFs are all independent. Therefore, the variance decomposition-based GSA method can apply to a BN. The CPFs can be the same where the probabilities are evaluated using the same model as in a parallel system.

From a Bayesian network, the SPF in Eq. (4) can be decomposed into subfunctions as

$$P_F^{sys} = g_0 + \sum_{i \in U} g_i + \sum_{i,j \in U, i < j} g_{ij} + \dots + g_{ij\dots m} \quad (8)$$

where the set of all m indices is denoted as $U = \{i, j, \dots, m\}$, and g 's are subfunctions. The subscripts in a subfunction represent the CPFs involved in the function. The subfunctions are defined as

$$g_0 = \int_0^1 P_F^{sys} \prod_{i \in U} f(P_F^i) dP_F^i \quad (9)$$

$$g_{ij\dots r} = \int_0^1 P_F^{sys} \prod_{k \notin U_{ij\dots r}} f(P_F^k) dP_F^k - \sum_{k \in U_{ij\dots r}} g_k - \sum_{k,l \in U_{ij\dots r}, k < l} g_{kl} - \dots - g_0 \quad (10)$$

where the set of indices corresponding to the sub-function is denoted as $U_{ij\dots r} = \{i, j, \dots, r\} \subset U$. For example, g_0 of Eq. (8) for Eq. (3) is obtained simply by replacing each CPF by its mean, and the first-order terms are also calculated by replacing all other

CPF than the CPF with the corresponding subscript by their means

$$g_0 = E[P_4(1 - P_2)(1 - P_1) + P_5(1 - P_3)P_1 + P_6P_2(1 - P_1) + P_7P_3P_1] \quad (11)$$

$$g_i = P_F^{sys}(E[P_1], \dots, E[P_{i-1}], P_i, E[P_{i+1}], \dots, E[P_7]) - g_0 \quad \forall i \quad (12)$$

Based on the normality assumption, the probability density function $f(P_F^k)$ of a CPF is a normal distribution in this paper.

The advantage of the decomposition in Eq. (8) is that the variance of SPF can be calculated as the sum of the variance of individual subfunctions as below. Such calculation is possible because the subfunctions are orthogonal to each other. Also, the variance of a subfunction is called partial variance [24]

$$V_F^{sys} = \sum_{i \in U} V[g_i] + \sum_{i,j \in U, i < j} V[g_{ij}] + \dots + V[g_{12\dots m}] \quad (13)$$

Each term in Eq. (13) can be calculated as

$$V_F^{sys} = \int_0^1 (P_F^{sys})^2 \prod_{k \in U} f(P_F^k) dP_F^k - g_0^2 \quad (14)$$

$$V[g_{ij\dots r}] = \int_0^1 g_{ij\dots r}^2 \prod_{k \in U_{ij\dots r}} f(P_F^k) dP_F^k - g_0^2 \quad (15)$$

It is noted that the subfunction g_i is a function of the i th CPF, $g_i(P_F^i)$, while g_{ij} is that of the i th and j th CPFs, $g_{ij}(P_F^i, P_F^j)$. Since a subfunction is a function of CPFs, the variance of a subfunction in Eq. (10) can be expressed in terms of the variances of CPFs as

$$V[g_{ij\dots r}] = \sum_{k \in U_{ij\dots r}} a_k V_F^k + \sum_{k,l \in U_{ij\dots r}, k < l} b_{kl} V_F^k V_F^l + \dots \quad (16)$$

where V_F^k is the variance of k th CPF. Therefore, from Eq. (13), the variance of SPF can also be expressed in terms of the variances of CPFs as

$$V_F^{sys} = \sum_{k \in U} \alpha_k V_F^k + \sum_{k,l \in U, k < l} \beta_{kl} V_F^k V_F^l + \dots + \gamma V_F^1 V_F^2 \dots V_F^m \quad (17)$$

where α_m is the sum of all linear terms of the variances of subfunctions, while β_{mm} is that of quadratic terms and so on.

Then, it is possible to define a sensitivity index. A sensitivity index with one subscript is referred to as the main sensitivity index because it shows the effect of the corresponding variable alone, and a sensitivity index with more than one subscript is referred to as an interaction sensitivity index because it shows the interaction effect among the corresponding variables. The sensitivity index is defined as

$$S_{ij\dots r} = \frac{V[g_{ij\dots r}]}{V_F^{sys}} \quad (18)$$

Using the sensitivity indices, the total sensitivity index is defined as the sum of the main sensitivity index and the interaction sensitivity indices. The total sensitivity index shows the total effect of the variance of a CPF on the variance of the SPF as

$$S_{Ti} = S_i + \sum S_{i,int} \quad (19)$$

where $S_{i,int}$ represents any interaction sensitivity index of which subscript possesses i .

4 Design Sensitivity Under Epistemic Uncertainty

The conservative SPF in Eq. (7) depends on design variables in the component as well as the number of samples used to calculate CPFs. Therefore, to control the reliability constraint, it would be necessary to establish the relationship between the conservative SPF and component design variables and the number of samples. Such relationship can be addressed in terms of design sensitivity in this section.

The sensitivity of an SPF can be derived using the chain rule of differentiation. Let d_{ij} be the j th design variable of the i th CPF. Then, the conservative SPF can be differentiated as

$$\begin{aligned} \frac{\partial P_{F,\text{cons}}^{\text{sys}}}{\partial d_{ij}} &= \frac{\partial (P_F^{\text{sys}} + z_{1-\alpha} \sigma_F^{\text{sys}})}{\partial d_{ij}} \\ &= \frac{\partial P_F^{\text{sys}}}{\partial P_F^i} \frac{\partial P_F^i}{\partial d_{ij}} + z_{1-\alpha} \frac{\partial \sigma_F^{\text{sys}}}{\partial V_F^{\text{sys}}} \frac{\partial V_F^{\text{sys}}}{\partial V_F^i} \frac{\partial V_F^i}{\partial P_F^i} \frac{\partial P_F^i}{\partial d_{ij}} \end{aligned} \quad (20)$$

Each term on the right-hand side of Eq. (20) can be calculated as follows. The first term, $\partial P_F^{\text{sys}} / \partial P_F^i$, can be obtained by differentiating the SPF from the Bayesian network model in Eq. (4). Since d_{ij} is only involved in the i th component, it is enough to consider the i th component only. Assuming that N_i samples are used to evaluate P_F^i , the derivative of CPF $\partial P_F^i / \partial d_{ij}$ can be obtained by differentiating the MCS approximation in Eq. (1) using Leibniz's rule as

$$\frac{\partial P_F^i(\mathbf{d})}{\partial d_{ij}} = \frac{1}{N_i} \sum_{k=1}^{N_i} I_F(h(\mathbf{d}, \mathbf{x}_k) \geq 0) s(\mathbf{x}_k; \mathbf{d}) \quad (21)$$

where $s(\mathbf{x}_k; \mathbf{d})$ is the partial derivative of the log-likelihood function with respect to its argument. The function is referred to as a score function [25]. The derivative of σ_F^{sys} with respect to V_F^{sys} can be calculated from the relationship between the standard deviation and variance as

$$\frac{\partial \sigma_F^{\text{sys}}}{\partial V_F^{\text{sys}}} = \frac{1}{2\sigma_F^{\text{sys}}} \quad (22)$$

Using the relationship in Eq. (5), the component variance can be differentiated with respect to the CPF as

$$\frac{\partial V_F^i}{\partial P_F^i} = \frac{1 - 2P_F^i}{N_i} \quad (23)$$

Therefore, all terms in Eq. (20) can be calculated except for the term, $\partial V_F^{\text{sys}} / \partial V_F^i$, which requires the relationship between the system variance and component variances. This term will be derived using GSA. The derivative of the variance of the SPF with respect to the variance of a CPF is calculated from Eq. (17) as

$$\begin{aligned} \frac{\partial V_F^{\text{sys}}}{\partial V_F^i} &= \alpha_i + \sum_{k \in U - U_{ij,r}} \beta_{ki} V_F^k \dots \sum_{k \in U - U_{12,i}} \beta_{ik} V_F^k \dots \\ &+ \gamma V_F^1 \dots V_F^{i-1} V_F^{i+1} \dots V_F^m \equiv \kappa_i \end{aligned} \quad (24)$$

Using Eqs. (21)–(24), the sensitivity in Eq. (20) can be rewritten as

$$\frac{\partial P_{F,\text{cons}}^{\text{sys}}}{\partial d_{ij}} = \frac{\partial P_F^i(\mathbf{d})}{\partial d_{ij}} \left(\frac{\partial P_F^{\text{sys}}}{\partial P_F^i} + z_{1-\alpha} \frac{\kappa_i (1 - 2P_F^i)}{2N_i \sigma_F^{\text{sys}}} \right) \quad (25)$$

Because κ_i is the sum of α_i and high order terms, Eq. (24) is not simple enough to calculate. In other words, both the main effect and the interaction effect must be considered to calculate the sensitivity. From Eq. (17), however, it is possible to formulate the total sensitivity index as

$$S_{Ti} = \frac{V(g_i) + V(g_{ij}) + \dots + V(g_{ij\dots il})}{V_F^{\text{sys}}} = \frac{\kappa_i V_F^i}{V_F^{\text{sys}}} \quad (26)$$

Therefore, the derivative can be simply expressed as

$$\frac{\partial V_F^{\text{sys}}}{\partial V_F^i} = \frac{S_{Ti} V_F^{\text{sys}}}{V_F^i} \quad (27)$$

Substituting Eq. (25) with Eq. (27), the sensitivity of a conservative estimate of the SPF with respect to the j th design variable of the i th component can be obtained as

$$\frac{\partial P_{F,\text{cons}}^{\text{sys}}}{\partial d_{ij}} = \frac{\partial P_F^i(\mathbf{d})}{\partial d_{ij}} \left(\frac{\partial P_F^{\text{sys}}}{\partial P_F^i} + z_{1-\alpha} \frac{S_{Ti} \sigma_F^{\text{sys}} (1 - 2P_F^i)}{2N_i V_F^i} \right) \quad (28)$$

Likewise, the sensitivity of the conservative estimate with respect to the number of samples in the i th component can be assessed using the chain rule of differentiation as

$$\frac{\partial P_{F,\text{cons}}^{\text{sys}}}{\partial N_i} = -z_{1-\alpha} \frac{S_{Ti} \sigma_F^{\text{sys}}}{4N_i \sigma_F^i} \quad (29)$$

Note that the sensitivity is always negative because the increasing number of samples will reduce the sampling uncertainty.

5 Effect of Sampling Uncertainty on System-Level Design Sensitivity

To demonstrate the effect of sampling uncertainty on sensitivity and to show in what situation the approximation of the sensitivity given as Eq. (28) can be used, the following two-node Bayesian network is considered. In the network, node B depends on node A, and the probability table corresponding to each marginal and conditional probability of failure is provided on the left side of the directed acyclic graph. ‘‘S’’ and ‘‘F’’ denote ‘‘Success’’ and ‘‘Failure,’’ respectively.

From the Bayesian network provided in Fig. 3, the SPF, which is defined as the probability of component B to fail, can be calculated as

$$P_F^{\text{sys}} = P_F^1 P_F^2 + (1 - P_F^1) P_F^3 \quad (30)$$

The confidence level is set to 90%, which corresponds to $z_{0.9} = 1.28$. Using the variance decomposition, the subfunctions and partial variances are calculated. Note that the subfunction g_{23} that represents the interaction between P_F^2 and P_F^3 as well as g_{123} that shows the interaction of all the CPFs is equal to zero because no term involves P_F^2 and P_F^3 together. Using the decomposition result, the coefficients in Eq. (17) are calculated. The probability of failure is calculated through the sampling method.

To show the accuracy of the sensitivity calculation, it is assumed that the conditional probabilities of failure in Fig. 3 are obtained using 1000 samples, where individual CPFs are $P_F^1 = 7.2\%$, $P_F^2 = 5.8\%$, and $P_F^3 = 1.0\%$. Thus, the first component is the least safe among the three.

Table 1 verifies the design sensitivity in Eq. (27), while comparing it with the result when the main sensitivity index is used instead of the total sensitivity index. As shown in the table, Eq. (27) holds for all the CPFs. On the other hand, the result is also satisfactory when the main sensitivity index is used to approximate the design sensitivity. The difference is less than 3% in this study when compared to κ_i , which is the true design sensitivity from Eq. (24). Still, the total sensitivity index will be used since it does not require any approximation.

The effect of sampling uncertainty on the sensitivity analysis is found in Eq. (28). In Table 2, the effect of design change on the probability calculation, $f' = \partial P_F^{\text{sys}} / \partial P_F^i$, is compared with the

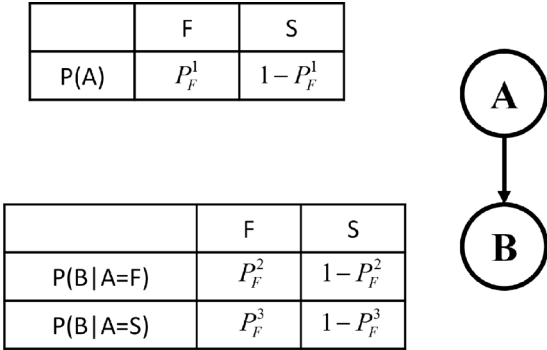


Fig. 3 Two-node Bayesian network

effect of uncertainty, $\sigma' = z_{1-\alpha} S_{Ti} \sigma_F^{sys} (1 - 2P_F^i) / 2N_i V_i$. f' represents the effect of design change on conservative SPF, while σ' represents the effect of sampling uncertainty.

Table 2 displays the consequence of incorporating the epistemic uncertainty with sensitivity analysis. In the case of P_F^3 , the sensitivity ratio is about 19%. Furthermore, σ' is linearly proportional to the confidence level. Therefore, the effect of uncertainty becomes considerable as the confidence level becomes high.

σ' relies on Eq. (27). Since the GSA is performed before the design sensitivity analysis, it is possible to compare the relative magnitude of σ' of each component as seen in Table 2. Table 3 compares the total sensitivity index of three CPFs. As seen in the table, S_{T3} is the largest, while S_{T1} is only 0.0171. In this regard, the sensitivity analysis corresponding to P_F^3 demonstrates that it is necessary to include the sampling uncertainty as in Table 2, while the total sensitivity index must be used for the sensitivity calculation as the authors pointed out in Table 1.

Table 4 shows the sensitivity results of the conservative estimate of the SPF with respect to the number of samples in each component. In the table, it is confirmed that $\partial P_{F,cons}^{sys} / \partial N_3$ possesses the largest value, whose corresponding total sensitivity index is also the largest.

6 Reliability-Based Design Optimization Under Sampling Uncertainty

To demonstrate the optimization procedure of a system under sampling epistemic uncertainty, a pyro-mechanical device (PMD) example is considered in this section. Based on the mathematical models described in Appendix, a Bayesian network is built first, as shown in Fig. 4. The probability table corresponding to each marginal and conditional probability of failure is provided next to the directed acyclic graph. “S” and “F” denote “Success” and “Failure,” respectively. There are two initiators connected in parallel to ensure a high reliability, and thus, the Bayesian network consists of three nodes. However, one of the initiators has a shorter heating element due to geometrical restriction in the device, therefore, the probabilities of failure are different for the two initiators. The probabilities are estimated by MCS using random input variables shown in Table 5. All the random variables follow a normal distribution. The standard deviations are fixed during the optimization. Note that the design variable is the mean

Table 1 Comparison of design sensitivity

CPF	P_F^1	P_F^2	P_F^3
(1) $S_i V_{tot} / V_i$	2.3040×10^{-3}	5.1840×10^{-3}	8.6118×10^{-1}
(2) $S_{Ti} V_{tot} / V_i$	2.3685×10^{-3}	5.2508×10^{-3}	8.6125×10^{-1}
(3) κ_i	2.3685×10^{-3}	5.2508×10^{-3}	8.6125×10^{-1}
(1)/(3) $\times 100$	97.27%	98.72%	99.99%
(2)/(3) $\times 100$	100%	100%	100%

Table 2 Effect of sampling uncertainty on sensitivity analysis

CPF	P_F^1	P_F^2	P_F^3
f'	0.048	0.072	0.928
σ'	4.697×10^{-4}	9.932×10^{-4}	0.1814
σ' / f'	0.97%	1.37%	19.54%

Table 3 Sensitivity index of CPF

Main sensitivity index	S_1	S_2	S_3		
	0.0171	0.0316	0.951		
Interaction sensitivity index	S_{12}	S_{13}	S_{23}	S_{123}	
	4.071×10^{-4}	7.377×10^{-5}	0	0	
Total sensitivity index	S_{T1}	S_{T2}	S_{T3}		
	0.0176	0.0320	0.951		

of a random variable, and Table 5 specifies the bounds of the design variables.

Since the piston moves if and only if the initiator works, the probability of failure of the piston when both of the initiators fail $P(Y = F | I_1 = F, I_2 = F)$ is one. Also, the performance of Pyrolock will be the same if one of the two initiators is successful or both of them are successful. Therefore, the three conditional probabilities $P(Y = F | I_1 = S, I_2 = S)$, $P(Y = F | I_1 = S, I_2 = F)$, and $P(Y = F | I_1 = F, I_2 = S)$ are the same.

From the Bayesian network provided in Fig. 4, the system probability of failure, which is defined as the probability of failure of the Pyrolock, can be calculated as

$$P_F^{sys} = P_Y + P_{I1}P_{I2} - P_{I1}P_{I2}P_Y \quad (31)$$

The confidence level is set to 95%, which corresponds to $z_{0.95} = 1.645$.

Before carrying out optimization, the accuracy of SPF in the Bayesian network is verified by comparing it with all-in-one MCS. First, a design point $\mathbf{d} = \{6, 1, 13, 1.5, 8.4E - 06\}$ is selected, which will not yield a zero probability of failure. Then, 20,000 samples are generated from the distribution of random input variables. For the Bayesian network, these 20,000 input samples are applied for each component model in Appendix to calculate the CPF first, and the SPF is obtained by using Eq. (31). The same 20,000 input samples are then recycled to calculate the SPF without using the Bayesian network. That is, the same 20,000 samples are applied to the mathematical models in Appendix to calculate 20,000 samples of moving distances of the piston from which the number of samples whose moving distance is less than 3 mm is counted. With the Bayesian network, the CPFs are estimated as $P_{I1} = 52.11\%$, $P_{I2} = 51.53\%$, and $P_Y = 17.30\%$. The corresponding SPF is equal to $P_F^{sys} = 40.27\%$. Without the Bayesian network, the SPF is estimated as $P_F^{sys} = 40.25\%$. The small difference is due to the numerical error in calculation.

The calculation is repeated for 10,000 times to verify that Eq. (31) estimates the SPF correctly without bias. The result shows that the mean of SPF from the Bayesian network and the MCS is exactly same as $E[P_F^{sys}] = 40.99\%$. Thus, Eq. (31) predicts SPF quite correctly. However, there is a small difference in the standard deviation of the SPF. The Bayesian network results in $E[\sigma(P_F^{sys})] = 0.0032$, while the MCS gives $E[\sigma(P_F^{sys})] = 0.0035$. There is a difference even though very small. This is because

Table 4 Sensitivity analysis results with respect to number of samples

	$\partial P_{F,cons}^{sys} / \partial N_1$	$\partial P_{F,cons}^{sys} / \partial N_2$	$\partial P_{F,cons}^{sys} / \partial N_3$
Sensitivity	-2.071×10^{-6}	-4.153×10^{-6}	-2.899×10^{-4}

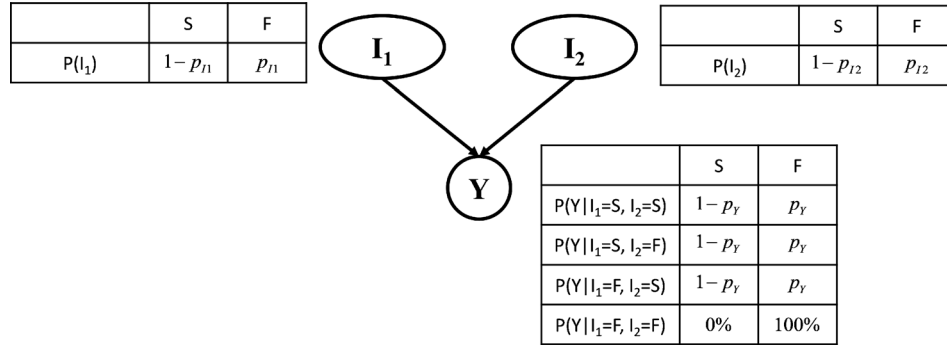


Fig. 4 Bayesian network of PMD system

Table 5 Random variables in PMD system

Component	Variable	Lower limit	Upper limit	Standard deviation
Initiator (I_1)	Heating element length (d_1)	2.0 (mm)	10.0 (mm)	1 (mm)
	Heating element diameter (d_2)	0.1 (mm)	2.0 (mm)	0.2 (mm)
Initiator (I_2)	Heating element length (d_3)	15.0 (mm)	20.0 (mm)	1 (mm)
	Heating element diameter (d_4)	0.1 (mm)	2.0 (mm)	0.2 (mm)
Piston (Y)	ZPP mass (d_5)	5×10^{-6} (kg)	15.5×10^{-6} (kg)	2.5×10^{-7} (kg)

when the Bayesian network is built up, it is assumed that $P(Y = F|I_1 = S, I_2 = S)$ is equal to $P(Y = F|I_1 = F, I_2 = S)$ and $P(Y = F|I_1 = S, I_2 = F)$. Therefore, when using a sample for P_Y , the sample adds information to three individual CPFs in the Bayesian network. However, it is concluded that the Bayesian network accurately estimates the system probability of failure with its uncertainty.

The optimization problem is formulated using a cost model to consider the effect of both the design variables and the number of samples. The cost model is composed of the operation cost and the design cost. The operation cost of the initiator is proportional to the volume of the heating element. There are two initiators, therefore, the operation cost is the sum of the two. Also, the operation cost of the piston model increases if the mass or density of the charge increase. The design cost is a multilinear function of the number of samples.

In general, the reliability constraint can be defined for both the components and the system. Although the system probability of failure is the target, still it is necessary to set the limit for each component probability of failure. Otherwise, the algorithm makes some of the component probabilities extremely high or low, which is undesirable. The sensitivity of the conservative estimate of CPF can be found in the paper by Bae et al. [9]. The optimization problem can then be formulated using the operation and the design costs as

$$\begin{aligned}
 \min \text{cost}(\mathbf{d}) &= \text{operation cost} + \text{design cost} \\
 &= \left[C_1 \left(\frac{(d_1 - 6)^2}{10} + \frac{(d_2 - 1)^2}{5} \right) + C_2 \left(\frac{(d_3 - 18)^2}{7} + \frac{(d_4 - 1)^2}{3} \right) \right] \\
 &+ C_3 d_5 + C_4 (n_1 + n_2) + C_5 n_3 \\
 \text{s.t. } &P[h_i(\mathbf{x}) > 0] + z_{0.95} \sigma_{P_i} < P_{T,i}, \quad i = 1 \sim 3 \\
 &P_F^{\text{sys}} + z_{0.95} \sigma_F^{\text{sys}} < P_{T,\text{sys}}, \\
 &\mathbf{d}^L \leq \mathbf{d} \leq \mathbf{d}^U, \quad \mathbf{d} \in \mathbf{R}^6 \text{ and } \mathbf{X} \in \mathbf{R}^6
 \end{aligned} \tag{32}$$

where $C_1 = 10$, $C_2 = 5$, $C_3 = 1$, $C_4 = 0.1$, and $C_5 = 0.2$ are used in the objective function. A scaled variable $n_i = N_i/10,000$ is used for normalization. The target probability of each component $P_{T,i}$ ($i = 1 \sim 3$) is set to 5%. Also, the system level target

probability $P_{T,\text{sys}}$ is 5%. The three component-level constraint functions are given as

$$\begin{aligned}
 h_1(\mathbf{x}) &= 350[^\circ\text{C}] - T_{I1}(\mathbf{x}; t = 0.005) > 0 \\
 h_2(\mathbf{x}) &= 350[^\circ\text{C}] - T_{I2}(\mathbf{x}; t = 0.005) > 0 \\
 h_3(\mathbf{x}) &= 0.003 - d_P[m] > 0
 \end{aligned} \tag{33}$$

The first two constraints are the failure of two initiators, while the last constraint defines the failure of the piston. The maximum number of available samples per each iteration is 10,000. Table 6 shows the information of the initial design variables, and Tables 7 and 8 summarize the RBDO results.

The result using 10,000 samples is shown in Table 8. At the optimum point, the probabilities of failure of all three components, as well as that of the system, are calculated. As expected, the conservative estimate of the CPF and SPF attains the target probability of failure. All the probabilities are conservative, meaning the CPFs at the optimum are lower than the target probability. The cost of the initial design is 8.4943, and at the optimum, it is slightly increased to 12.4374. It is because the initial design is in the infeasible region. As more samples are provided, the optimum design will be closer to that of the traditional RBDO because the sampling uncertainty will diminish as shown in Eqs. (28) and (29).

Note that more samples are provided to the first initiator than the second initiator although the design cost is same for both. This is because the optimum design is found on the design limit. In other words, the algorithm tries to attain the target probability of failure by reducing the uncertainty of the design. Also, the least number of samples is given to evaluate the CPF of the piston since the relative cost of the sample is expensive and the cost function corresponding to the sampling of the piston is linear.

Table 6 Initial design of Pyrolock

Component	Variable	Value	Variable	Value	Variable	Value
I_1	d_1	5.00 (mm)	d_2	0.30 (mm)	n_1	0.5
I_2	d_3	17.00 (mm)	d_4	0.40 (mm)	n_2	0.5
Y	d_5	5×10^{-6} (kg)			n_3	0.5

Table 7 Optimization results of Pyrolock

Component	Variable	Value	Variable	Value	Variable	Value
I_1	d_1	6.18 (mm)	d_2	0.10 (mm)	n_1	0.4255
I_2	d_3	18.06 (mm)	d_4	0.31 (mm)	n_2	0.2378
Y	d_5	9.92×10^{-6} (kg)			n_3	0.1012

Table 8 Probability of failure at optimum

Component	Probability of failure	Conservative estimate
I_1	4.25%	4.76%
I_2	4.25%	4.93%
Y	3.56%	4.52%
System	3.73%	4.69%

The optimization shows that the number of samples also can be adjusted during the iteration to satisfy the target probability. This is an important issue when the cost of model evaluation, which is expressed as design cost in this problem, is high. Moreover, the number of samples at the optimum can be used for model validation. Note that the constraints used in the algorithm are mathematical models that mimic the physical behavior of the component. Therefore, the validation should be carried out with the experiments. For that purpose, it is only required to do the same number of experiments as the samples to validate the result according to the optimization rather than carrying out the same number of experiments on all the components, which significantly reduces the cost.

Conclusions

This paper presented how to include sampling uncertainty in the RBDO of a system using the Bayesian network. The design sensitivity of the conservative estimate of probability with respect to the design variables and the number of samples is derived using global sensitivity analysis along with the Bayesian network. This paper shows how the global sensitivity analysis can be applied to design sensitivity analysis, rather than using it only for screening insignificant variables. The result shows that both changing design and changing the number of samples can be used to satisfy the target probability of failure in RBDO under sampling uncertainty. Moreover, the paper demonstrates that it is necessary to compare the total sensitivity index to decide when to include the sampling uncertainty in the design sensitivity analysis. If small, sensitivity calculation may ignore the sampling uncertainty.

In this paper, MCS is applied to explain the methodology. Although sampling methods are expensive, a lot of industry still rely on a sampling method because of errors in approximate methods. Because sampling methods are expensive, the paper makes more sense as we consider sampling uncertainty. Having said that, other methods can also be utilized as long as CPFs, and their uncertainty can be estimated. Once the CPFs are estimated, the rest of the procedure does not require much computational cost. Besides, computational resource problem can be solved by replacing the model with a surrogate model such as Kriging with which reliability-based design optimization is often performed. Once a surrogate model with enough accuracy is available, there is not much difference in computational effort for different methods. The effect of the accuracy of surrogate model (i.e., surrogate model uncertainty) on the proposed method will be addressed in the future research.

Acknowledgment

Agency for Defense Development and Defense Acquisition Program Administration of the Korean government supported this research.

Funding Data

- Agency for Defense Development (Defense Acquisition).

Nomenclature

- $A_{c,tot}$ = total particle surface area
- A_{ps} = cross-sectional area of piston
- A_e^{surf} = surface area
- C_p = heat capacity
- \mathbf{d} = design variable
- d_e = diameter of heating element
- d_{ij} = j th design variable in i th component-level probability of failure
- f = probability density function
- F_{ba} = ball friction
- F_{or} = o-ring friction
- F_{sh} = shear pin force
- g = subfunction
- h = limit state function
- I = input current
- I_F = indicator function
- l_e = length of heating element
- l_{pin} = pin length
- m_{ba} = ball mass
- m_c = charge mass
- m_{ps} = piston mass
- N_i = number of samples to calculate P_F^i
- P_F = probability of failure
- $P_{F,cons}$ = conservative estimate of probability of failure
- P_{ps} = chamber pressure
- P_T = target probability of failure
- P_F^{sys} = system probability of failure
- P_F^i = the i th component-level probability of failure
- Q_{loss} = heat transfer
- R = resistance of heating element
- r_b = burning rate
- R_g = universal gas constant
- r_w = resistivity
- s = score function
- S_i = sensitivity index
- S_{int} = interaction sensitivity index
- S_{Ti} = total sensitivity index
- T = temperature
- T_g = gas flame temperature
- T_{pin} = temperature at the end of pin
- T_0 = ambient temperature
- V = variance
- V_{ps} = chamber volume
- \mathbf{X} = random variable
- y_{th} = threshold value of y
- $z_{1-\alpha}$ = $1 - \alpha$ level z-score
- γ = specific heat ratio
- ε = emissivity
- e = burning distance
- η_p = correction factor
- κ = conductivity
- ρ_c = charge density
- σ = standard deviation
- σ_s = Stefan–Boltzmann constant
- v_{ps} = piston velocity

Appendix

Overview of Pyro-Mechanical Device

Pyro-mechanical device represents a group of mechanical devices, which obtain the required energy from chemical reactions. It is widely used in the field of aeronautics such as launching, initiating, controlling, and separating the missiles, space shuttle bodies,

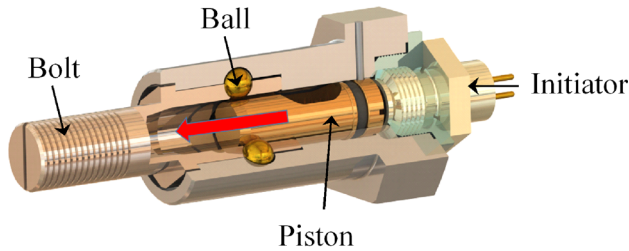


Fig. 5 Pyrolock device

and satellites [26]. Because the device is initiated by chemical reactions, it is normally disposable. Thus, it is not possible to test a PMD that is already assembled into a system. Moreover, this one-shot device is usually stored for a long period in nominal condition and then initiated. For this reason, the target probability of failure must be low.

Figure 5 shows an example of PMD, a so-called Pyrolock. The device holds two structures through the bolt at the end, and it releases the outer structure by dropping the balls once it receives an electric signal through the initiator. During the initiation, a copper heating element undergoes Joule heating. When the temperature of the bridge is sufficiently elevated, an explosive charge is detonated. The rapidly expanding explosive pushes the piston forward. When the piston is sufficiently advanced, the metal balls drop into awaiting slots in the piston. The bolt may then separate from the Pyrolock.

There are multiple failure modes possible for this device due to the many part dependencies. In this example, the model is simplified to consider only two failure modes: the failure of the copper bridge and the failure of the piston. The failure of the copper bridge is defined as the temperature being less than 350 °C when 3.5 A current is applied for 5 ms. The failure of the piston is defined as the moving distance of the piston is less than the diameter of the ball, which is 6 mm when the piston stops. Figure 6 demonstrates possible failures in each component. On the left of Fig. 6, the temperature of the copper bridge in the initiator does not reach 350 °C within 5 ms, and on the right side, the piston proceeds no more than 1900 μm when it stops while at least 3000 μm of displacement is required in order to successfully operate the PMD system. Although the example is simple, it is still enough to demonstrate the effect of epistemic uncertainty on the optimization.

Pyro-Mechanical Device Model Description

Each component of the PMD system is modeled as a system of differential equations to describe the physical behavior of the component. First, the temperature rate of the heating element can be modeled as an ordinary differential equation as

$$\frac{dT}{dt} = \frac{1}{C_p} \left[I^2 R(T) - \frac{\pi \kappa d_e^2 (T - T_{pin})}{2l_{pin}} - \epsilon \sigma_s A_e^{surf} (T^4 - T_0^4) \right] \quad (A1)$$

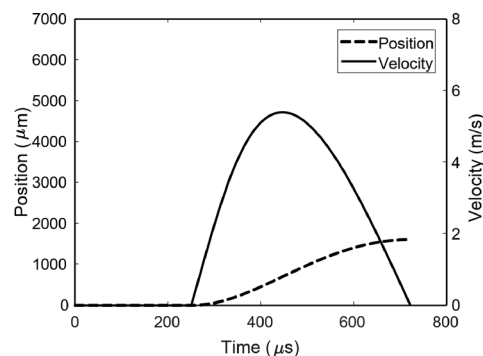
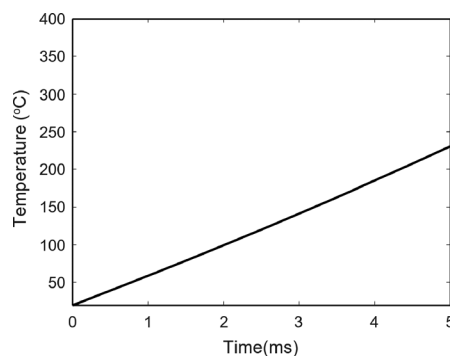


Fig. 6 Failure modes in Pyrolock

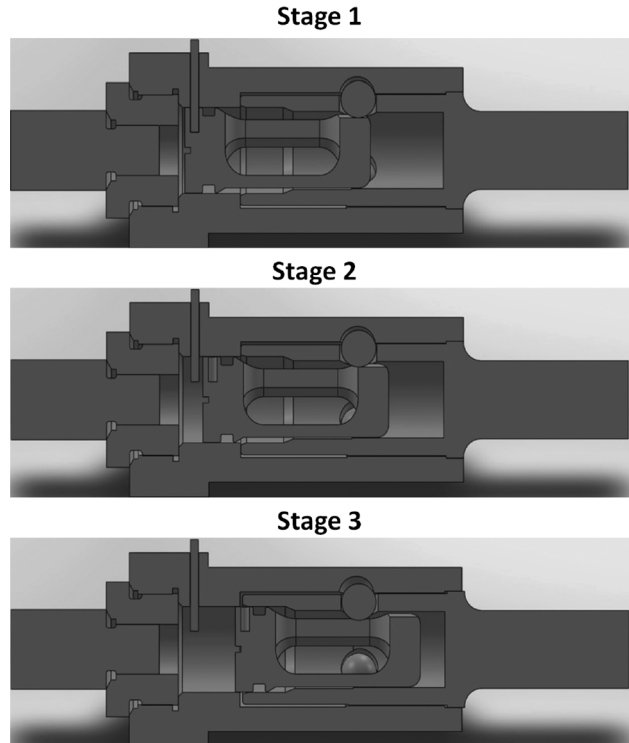


Fig. 7 Motion of piston in each stage

where the resistance and resistivity are, respectively, defined as

$$R(T) = 0.0005 \frac{l_e}{d_e^2} r_w(T) \quad (A2)$$

$$r_w(T) = 40.604 + 0.06984T \quad (A3)$$

As the temperature rises by Joule heating, heat is transferred to the surface of the element through conduction and radiation. The second and third terms of Eq. (A1) represent such transfer. Note that the resistivity also increases as the temperature rises. Other variables in the equations are explained in Nomenclature.

The motion of the piston is staged in three steps. During stage 1, chemical reactions in the initiator generate energy in the form of pressure in the chamber, which is the main driving force to the piston. Initially, the location of the piston is fixed by a shear pin. When the pressure in the chamber is large enough to break the shear pin, the piston starts its motion. A possible failure occurs when the pressure is insufficient so that the pin remains secure.

While the piston is moving, there exist resistive forces from the O-ring and the ball bearing. Stage 2 simulates the motion of the piston under the pressure in the chamber, O-ring force, and ball

friction until the ball bearings are dropped to the hollow space in the piston. In this system, it is considered that the ball bearings are dropped if the piston moves more than the diameter of the ball bearings, which is 3 mm. Stage 3 simulates the motion of piston after the ball bearings are dropped, where the ball friction no more applies to the motion of the piston. The model calculates the motion of the piston and the change of the pressure as a function of time. The following system of differential equations describes the chemical reactions and the motion of piston:

$$\frac{d\rho_c}{dt} = \frac{1}{V_{ps}} \left[\frac{dm_c}{dt} - \rho_c(A_{c,tot}r_b + A_{ps}v_{ps}) \right] \quad (A4)$$

$$\frac{dP_{ps}}{dt} = \frac{1}{V_{ps}} \left[\eta_p \frac{dm_c}{dt} R_g \gamma T_g - (\gamma - 1) \left(P_{ps} A_{ps} v_{ps} + \frac{dQ_{loss}}{dt} \right) - P_{ps} \frac{dV_{ps}}{dt} \right] \quad (A5)$$

$$\frac{dV_{ps}}{dt} = A_{c,tot}r_b + A_{ps}v_{ps} \quad (A6)$$

$$\frac{de}{dt} = r_b \quad (A7)$$

$$\frac{dv_{ps}}{dt} = \begin{cases} 0 & \text{(Stage 1)} \\ (P_{ps}A_{ps} - F_{or} - F_{ba})/m_{ps} & \text{(Stage 2)} \\ (P_{ps}A_{ps} - F_{or})/m_{ps} & \text{(Stage 3)} \end{cases} \quad (A8)$$

$$F_{sh} = \begin{cases} 234 & \text{(Stage 1)} \\ 0 & \text{(Stage 2, 3)} \end{cases} \quad (A9)$$

$$F_{or} = \begin{cases} 0 & \text{(Stage 1)} \\ -2.64E - 14P_{ps}^2 + 1.67E - 06P_{ps} + 14.04 & \text{(Stage 2, 3)} \end{cases} \quad (A10)$$

$$F_{ba} = \begin{cases} 0 & \text{(Stage 1)} \\ 3000 & \text{(Stage 2, 3)} \end{cases} \quad (A11)$$

Equations (A4) and (A5), respectively, represent the rate of charge density and the pressure. The pressure rate also considers the pressure loss by air resistance and volume change. Equation (A6) shows the volume rate as the piston moves forward and Eq. (A7) calculates the burning rate. Equation (A8) is the equation of motion of the piston under the shear pin force in Eq. (A9), O-ring force in Eq. (A10), and the friction force in Eq. (A11). Note that the forces are defined differently from a stage to another. This is because the piston undergoes different conditions when the stage changes. Equations (A4)–(A11) are solved simultaneously [19]. Figure 7 illustrates each stage.

References

- [1] Cadini, F., and Gioietta, A., 2016, "A Bayesian Monte Carlo-Based Algorithm for the Estimation of Small Failure Probabilities of Systems Affected by Uncertainties," *Reliab. Eng. Syst. Saf.*, **153**, pp. 15–27.
- [2] Howard, R. A., 1988, "Uncertainty About Probability: A Decision Analysis Perspective," *Risk Anal.*, **8**(1), pp. 91–98.
- [3] Mosleh, A., and Bier, V. M., 1996, "Uncertainty About Probability: A Reconciliation With the Subjectivist Viewpoint," *IEEE Trans. on Syst., Man, and Cybern. Part A: Syst. and Hum.*, **26**(3), pp. 303–310.
- [4] Reneke, J. A., Wiecek, M. M., Fadel, G. M., Samson, S., and Nowak, D., 2010, "Design Under Uncertainty: Balancing Expected Performance and Risk," *ASME J. Mech. Des.*, **132**(11), p. 111009.
- [5] Hofer, E., Kloos, M., Krzykacz-Hausmann, B., Peschke, J., and Wolterreck, M., 2002, "An Approximate Epistemic Uncertainty Analysis Approach in the Presence of Epistemic and Aleatory Uncertainties," *Reliab. Eng. Syst. Saf.*, **77**(3), pp. 229–238.
- [6] Choi, J., An, D., and Won, J., 2010, "Bayesian Approach for Structural Reliability Analysis and Optimization Using the Kriging Dimension Reduction Method," *ASME J. Mech. Des.*, **132**(5), p. 051003.
- [7] Nannapaneni, S., and Mahadevan, S., 2016, "Reliability Analysis Under Epistemic Uncertainty," *Reliab. Eng. Syst. Saf.*, **155**, pp. 9–20.
- [8] Bae, S., Kim, N. H., Park, C., and Kim, Z., 2017, "Confidence Interval of Bayesian Network and Global Sensitivity Analysis," *AIAA J.*, **55**(11), pp. 3916–3924.
- [9] Bae, S., Kim, N. H., and Jang, S. G., 2018, "Reliability-Based Design Optimization Under Sampling Uncertainty: Shifting Design Versus Shaping Uncertainty," *Struct. Multidiscip. Optim.*, **57**(5), pp. 1845–1855.
- [10] Grigoriu, M., 1982, "Methods for Approximate Reliability Analysis," *Struct. Saf.*, **1**(2), pp. 155–165.
- [11] Au, S. K., and Beck, J. L., 2001, "Estimation of Small Failure Probabilities in High Dimensions by Subset Simulation," *Probab. Eng. Mech.*, **16**(4), pp. 263–277.
- [12] Sheather, S. J., and Jones, M. C., 1991, "A Reliable Data-Based Bandwidth Selection Method for Kernel Density Estimation," *J. R. Stat. Soc. Ser. B Stat. Methodol.*, **53**(3), pp. 683–690.
- [13] Jensen, F. V., and Nielsen, T. D., 2007, *Bayesian Networks and Decision Graphs*, Springer Science & Business Media, New York.
- [14] Hu, Z., and Mahadevan, S., 2018, "Bayesian Network Learning for Data-Driven Design," *J. Risk Uncertain. Eng. Syst. Part B Mech. Eng.*, **4**(4), p. 041002.
- [15] Liang, C., and Mahadevan, S., 2016, "Multidisciplinary Optimization Under Uncertainty Using Bayesian Network," *SAE Int. J. Mater. Manuf.*, **9**(2), pp. 419–429.
- [16] Liang, C., and Mahadevan, S., 2017, "Pareto Surface Construction for Multi-Objective Optimization Under Uncertainty," *Struct. Multidiscip. Optim.*, **55**(5), pp. 1865–1882.
- [17] Jin, R., Chen, W., and Sudjianto, A., 2004, "Analytical Metamodel-Based Global Sensitivity Analysis and Uncertainty Propagation for Robust Design," *SAE Tech. Paper No. 2004-01-0429*.
- [18] Fraser, D. A. S., 1958, *Statistics-An Introduction*, John Wiley and Sons, New York, pp. 124–125.
- [19] Picheny, V., Kim, N. H., and Haftka, R. T., 2010, "Application of Bootstrap Method in Conservative Estimation of Reliability With Limited Samples," *Struct. Multidiscip. Optim.*, **41**(2), pp. 205–217.
- [20] Mahadevan, S., Zhang, R., and Smith, N., 2001, "Bayesian Networks for System Reliability Reassessment," *Struct. Saf.*, **23**(3), pp. 231–251.
- [21] Bichon, B. J., McFarland, J. M., and Mahadevan, S., 2011, "Efficient Surrogate Models for Reliability Analysis of Systems With Multiple Failure Modes," *Reliab. Eng. Syst. Saf.*, **96**(10), pp. 1386–1395.
- [22] Saltelli, A., 2004, "Global Sensitivity Analysis: An Introduction," 4th International Conference on Sensitivity Analysis of Model Output (SAMO'04), Santa Fe, NM, Mar. 8–11.
- [23] Jiang, Z., Chen, W., and German, B. J., 2016, "Multidisciplinary Statistical Sensitivity Analysis Considering Both Aleatory and Epistemic Uncertainties," *AIAA J.*, **54**(4), pp. 1326–1338.
- [24] Chen, W., Jin, R., and Sudjianto, A., 2005, "Analytical Variance-Based Global Sensitivity Analysis in Simulation-Based Design Under Uncertainty," *ASME J. Mech. Des.*, **127**(5), pp. 875–886.
- [25] Lee, I., Choi, K. K., and Zhao, L., 2011, "Sampling-Based RBDO Using the Stochastic Sensitivity Analysis and Dynamic Kriging Method," *Struct. Multidiscip. Optim.*, **44**(3), pp. 299–317.
- [26] Jang, S. G., Lee, H. N., and Oh, J. Y., 2014, "Performance Modeling of a Pyrotechnically Actuated Pin Puller," *Int. J. Aeronaut. Space Sci.*, **15**(1), pp. 102–111.